Charged and radially excited boson stars in anti–de Sitter spacetime

Yves Brihaye[*]

Service de Physique de l'Univers, Champs et Gravitation, Université de Mons, 7000 Mons, Belgium

Felipe Console[†]

Instituto de Física de São Carlos, Universidade de São Paulo, São Carlos, São Paulo 13560-970, Brazil

Betti Hartmann[‡]

Department of Mathematics, University College London, Gower Street,
London WC1E 6BT, United Kingdom

We study charged and radially excited boson stars in both asymptotically flat as well as asymptotically anti–de Sitter spacetime. We demonstrate that two different types of radially excited solutions exist: one that persists in the linear limit of small scalar fields, in which analytical arguments suggest the existence of these solutions, and one that appears only in the highly nonlinear regime of the model. We also demonstrate that the formation of wavy scalar hair discussed previously for black holes and boson stars in asymptotically flat spacetime persists for asymptotically anti–de Sitter spacetime.

I. INTRODUCTION

Anti–de Sitter (AdS)—together with Minkowski and de Sitter (dS)—spacetime plays an important role among known exact solutions of the Einstein equation. All three spacetimes are maximally symmetric, i.e., admit the largest possible amount of Killing vectors. Minkowski, dS, and AdS possess constant vanishing, positive, and negative curvature, respectively, with the Ricci scalar being proportional to the cosmological constant. Among these three spacetimes, AdS is special as it possesses a conformal boundary, i.e., a boundary that is in causal contact with the interior of the spacetime. As such, physics in the interior can be connected to (albeit different) physics on the boundary. The AdS/CFT correspondence [1] (or, more generally, the gauge-gravity correspondence [2]) as a prediction rooted in string theory uses exactly this idea: a gravity theory in d-dimensional AdS is dual to a conformal field theory on the $(d-1)$-dimensional boundary of AdS. The duality also predicts that there exists a weak-strong coupling duality between the theories in the bulk and on the boundary. Consequently, solutions to (weakly coupled) gravitational theories in d-dimensional asymptotically AdS (aAdS) have been used to make predictions about strongly coupled field theories in $(d-1)$ dimensions. One of the main examples that has

been widely studied are models for high-temperature superconductivity [3]. Using bulk black holes allows us to study the temperature dependence of the phase transition's order parameter, while phase transitions can also be modeled using solitonic objects [4]. The latter have no temperature ascribed to them, but phase transitions appear, e.g., when varying the chemical potential. Most discussions of these so-called "holographic superconductors" have been done using a scalar field in the bulk and consequently interpreting the value of this scalar field on the conformal boundary as the expectation value of an operator in the dual field theory with dimension equal to the power of the falloff of the scalar field in aAdS. In the language of condensed matter, these superconductors would correspond to s-wave superconductors.

Scalar fields are well motivated in particle physics models as well as effective descriptions of collective phenomena. Q-balls are lumps of complex scalar field carrying a conserved Noether charge that results from the invariance of the model under a U(1) gauge transformation [5]. They possess a scalar field that oscillates with constant frequency such that the energy-momentum tensor (and consequently the spacetime) stays static. These objects appear, e.g., in supersymmetric extensions of the Standard Model [6] and need specific scalar field potentials (with attractive and repulsive terms) in order to exist. In [7] an effective exponential potential that appears in gauge-mediated supersymmetric breaking has been discussed in this context. Boson stars [8–11] are the curved spacetime equivalent of Q-balls. Other than their flat spacetime

[*]yves.brihaye@umons.ac.be
[†]felipe.console@usp.br
[‡]b.hartmann@ucl.ac.uk

104058-1

counterparts, they do not require a higher-order scalar field potential, but exist for a non-self-interacting and massive scalar field. Boson stars also exist in aAdS spacetime [12], but now—in contrast to the asymptotically flat spacetime case—are no longer exponentially localized, but possess a power-law falloff for the scalar field function. The power of this falloff is determined by the mass and the angular frequency of the scalar field. The value of the scalar field on the conformal boundary can then be interpreted as the expectation value of a dual operator in the corresponding boundary field theory, e.g., as a glueball condensate [13].

Interesting new phenomena appear when gauging the U(1) symmetry, i.e., when electrically charging the boson star. This has been studied for a fourth-order scalar field potential [14], a V-shaped potential [15,16], an exponential potential [17], and a sixth-order potential [18], as well as for a massive scalar field with no self-interaction [19], respectively. When the gauge interaction becomes strong, charged boson stars cease to exist, which is related to the fact that the individual constituents, the scalar bosons, that make up the star are now also electrically charged and hence the electric repulsive force becomes important.

In this paper, we study charged boson stars in asymptotically flat and AdS spacetime, respectively. In the former case, which has been discussed in the literature previously, we show that radially excited charged boson stars exist and that these have very different qualitative properties as compared to the unexcited boson stars. In particular, we demonstrate that two disconnected branches of solutions exist. Radially excited boson stars have been discussed in the uncharged case before for nonrotating solutions [20–22] as well as rotating boson stars [20,23]. In these papers, it was shown that the excited solutions behave qualitatively very different as compared to the unexcited ones. This is also what we see in our work when charging the boson stars. We will elaborate on this in the following in more detail.

II. SETUP

We consider a U(1)-charged complex scalar field Ψ, minimally coupled to gravity with negative cosmological constant Λ and a scalar field potential $\mathcal{U}$. The action is given by

$$S = \int d^4x \sqrt{-g} \left(\frac{\mathcal{R}}{16\pi G} - \frac{\Lambda}{8\pi G} - (D_\mu \Psi)(D^\mu \Psi)^* \right.$$
$$\left. - \frac{1}{4} F_{\mu\nu} F^{\mu\nu} - \mathcal{U}(|\Psi|^2) \right), \tag{1}$$

where $\mathcal{R}$ is the Ricci scalar, G is Newton's gravitational constant, $D_\mu = \nabla_\mu + iqA_\mu$ is the gauge covariant derivative, A_μ is the U(1) gauge field, $F_{\mu\nu} = \partial_\mu A_\nu - \partial_\nu A_\mu$ is the field strength tensor, and q is the scalar charge.

The equations of motion are obtained by varying the action with respect to metric and the matter fields and read, respectively,

$$G_{\mu\nu} + \Lambda g_{\mu\nu} = 8\pi G T_{\mu\nu},$$
$$\nabla_\mu F^{\nu\mu} = iq(\Psi^*(D^\nu \Psi) - \Psi(D^\nu \Psi)^*) \equiv qj^\nu,$$
$$D_\mu D^\mu \Psi = \frac{d\mathcal{U}}{d|\Psi|^2} \Psi. \tag{2}$$

$G_{\mu\nu}$ is the Einstein tensor and the energy-momentum tensor $T_{\mu\nu}$ can be written as the sum of the energy momentum-tensor for the scalar field $T_{\mu\nu}^{(\Psi)}$ and for the electromagnetic field $T_{\mu\nu}^{(\mathrm{EM})}$ as follows:

$$T_{\mu\nu} = T_{\mu\nu}^{(\Psi)} + T_{\mu\nu}^{(\mathrm{EM})}, \tag{3}$$

with

$$T_{\mu\nu}^{(\Psi)} = (D_\mu \Psi)(D_\nu \Psi)^* + (D_\mu \Psi)^*(D_\nu \Psi)$$
$$- g_{\mu\nu}((D_\alpha \Psi)(D^\alpha \Psi)^* + \mathcal{U}),$$
$$T_{\mu\nu}^{(\mathrm{EM})} = F_{\mu\alpha} F_\nu^\alpha - \frac{1}{4} g_{\mu\nu} F_{\alpha\beta} F^{\alpha\beta}. \tag{4}$$

We consider a scalar self-interacting potential of the form

$$\mathcal{U}(|\Psi|^2) = \mu^2 \eta^2 \left(1 - \exp\left(-\frac{|\Psi|^2}{\eta^2} \right) \right), \tag{5}$$

where μ is the mass of the boson and η is an energy scale. This potential has been considered previously in the construction of Q-balls and boson stars in AdS [7,13]. Gauged boson stars with a sixth-order scalar field potential have been discussed in [18] and the qualitative features are very similar to those in the exponential case. That is why we do not investigate the sixth-order potential in more detail here because we believe this to be the case for the solutions discussed here too.

In the following, the spacetime is chosen to be static and spherically symmetric with adapted coordinates $\{t, r, \theta, \varphi\}$ such that $\xi = \partial_t$ and $\eta = \partial_\varphi$ are a time- and spacelike Killing vector, respectively. On the other hand, the ansatz for the matter fields is nonstatic since, although static solutions are not forbidden by Derrick's theorem when gauge fields are involved, static gauge fields with s vanishing A_t component lead to magnetic fields only and these cannot be spherically symmetric in Abelian gauge field theory (there are no monopole terms). However, we will choose an ansatz that will lead to a static energy-momentum tensor to be consistent with a static spacetime. The ansatz for the metric, scalar field Ψ, and U(1) gauge field A_μ then reads

$$ds^2 = -N(r)\sigma(r)^2 dt^2 + \frac{1}{N(r)}dr^2 + r^2 d\theta^2 + r^2 \sin^2\theta d\varphi^2,$$

$$\Psi = \Psi(t, r) = e^{-i\omega t}\psi(r), \qquad A_\mu dx^\mu = V(r)dt, \qquad (6)$$

where we will use $N(r) = 1 - 2m(r)/r$ with $m(r)$ a mass function. Replacing the above ansatz into (2) we obtain a system of four coupled nonlinear ordinary differential equations, which read

$$m' = \frac{1}{2}r^2\Lambda + 4\pi G r^2 \left(\mathcal{U} + \frac{(\omega - qV)^2}{N\sigma^2}\psi^2 + \frac{(V')^2}{2\sigma^2} + N(\psi')^2 \right),$$

$$\sigma' = \frac{8\pi G r}{N^2\sigma}((\omega - qV)^2\psi^2 + N^2\sigma^2(\psi')^2), \qquad (7)$$

$$\psi'' = -\left(\frac{N'}{N} + \frac{\sigma'}{\sigma} + \frac{2}{r} \right)\psi' - \frac{(\omega - qV)^2}{N^2\sigma^2}\psi + \frac{1}{N}\frac{d\mathcal{U}}{d|\Psi|^2}\psi,$$

$$V'' = -\left(\frac{2}{r} - \frac{\sigma'}{\sigma} \right)V' - \frac{2q(\omega - qV)}{N}\psi^2. \qquad (8)$$

The above equations obviously depend only on the gauge invariant combination $\omega - qV$, which also appears in the expression for the globally conserved Noether charge that reads

$$Q_N = \int_0^\infty dr \frac{2r^2\psi^2}{N\sigma}(qV - \omega). \qquad (9)$$

Q_N has often been interpreted as the number of bosonic particles of mass μ that make up the boson star. While in the ungauged case, next to the gravitational attraction, only the scalar field potential is responsible for repulsion between these individual constituents, there is an additional repulsive electric force acting in the gauged case. Hence, the properties of electrically charged boson stars are similar to those of the ungauged stars as long as the electric field is small, but deviate significantly when the gauge interaction becomes important.

In order to find globally regular solutions in an aAdS, we need to impose appropriate boundary conditions. Close to the origin $r = 0$, the equations of motion (7) and (8) imply that

$$m(0) = 0, \qquad \psi'(0) = 0, \qquad V'(0) = 0, \qquad (10)$$

while $\psi(0) \equiv \psi_0$, $\sigma(0) \equiv \sigma_0$, and $V(0) \equiv V_0$ are *a priori* free parameters. However, we can use the gauge freedom to fix $V(0) = 0$. The values ψ_0 and σ_0 will, on the other hand, be determined numerically.

Asymptotically, the leading terms of the metric functions are

$$N(r \to \infty) \sim 1 - \frac{\Lambda}{3}r^2, \qquad \sigma(r \to \infty) \sim 1, \qquad (11)$$

from which we can derive the behavior of the matter field functions. This becomes

$$V(r \to \infty) \sim \Phi - \frac{Q_e}{r}, \qquad \psi(r \to \infty) \sim \frac{\psi_+}{r^{\Delta_+}} + \frac{\psi_-}{r^{\Delta_-}},$$

$$\Delta_\pm = \frac{3}{2} \pm \frac{1}{2}\sqrt{9 - \frac{12\mu^2}{\Lambda}}, \qquad (12)$$

where Φ is a constant that we will often refer to as "the chemical potential" and Q_e is the electric charge of the solution that can be shown to be related to the Noether charge by $Q_e = eQ_N$. In fact, with our choice $V(0) = 0$, Φ denotes the electric potential difference between the origin and infinity.

Note that, different from the asymptotically flat space-time case, where ψ falls of exponentially,

$$\psi(r \to \infty) \sim \frac{\exp\left(-\sqrt{\mu^2 - (\omega - q\Phi)^2}r\right)}{r} \qquad (\Lambda = 0), \quad (13)$$

the scalar field now has a power-law falloff as long as $\mu^2 > 3\Lambda/4$. In the following, we will choose $\mu^2 > 0$, and since $\Lambda < 0$, this implies that Δ_- is negative and the corresponding solution to ψ would diverge as $r \to \infty$. For this reason we set $\psi_- = 0$ and consider only the regular solution at infinity, $\psi \sim \psi_+/r^{\Delta_+}$. ψ_+ is a constant that can then be interpreted as the expectation value of a "condensate" in the dual description on the conformal boundary.

Finally, the mass M of the solution can be read off from the asymptotic behavior of the mass function $m(r)$, which behaves as [12]

$$m(r \to \infty) \sim M + \frac{\Lambda r^3}{6} - \frac{2\pi G Q^2}{r} + n_1 r^{-2\Delta_+ + 3}, \qquad (14)$$

where n_1 is a constant depending on Λ and we need to subtract the diverging part for $\Lambda \neq 0$, which—more formally—would be done using the counterterm approach.

A. Radially excited solutions and gauged oscillons

Assuming ψ to be small we find the linearized scalar field equation

$$\frac{d}{dz}\left(z^2 f \frac{d\psi}{dz} \right) = \left(\mu^2 - \frac{\Omega^2}{f} \right)\ell^2 z^2\psi, \qquad f = 1 + z^2, \qquad (15)$$

where we have defined $z = r/\ell$ with $\ell = \sqrt{-3/\Lambda}$ as the AdS radius and $\Omega = \omega - q\Phi$. The solutions to this equation are so-called "oscillons" and have been discussed in the ungauged case before (see, e.g., [24–26]). Since the scalar field sources the U(1) gauge field only via a current proportional to ψ^2, the gauge field equation can be integrated to $V(r) \sim \Phi - Q_e/r$ in the limit of $\psi \ll 1$. The leading term of the gauge field inserted into the scalar

field equation is then $V \sim \Phi$, i.e., V equal to its chemical potential. Now, we will introduce

$$y = \frac{1}{1+z^2}, \qquad \psi = y^p F(y) \qquad (16)$$

to rewrite (15). This gives a hypergeometric equation of the form

$$y(y-1)\frac{d^2 F}{dy^2} + ((a+b+1)y - c)\frac{dF}{dy} + abF = 0, \quad (17)$$

with

$$a = p - \frac{\ell\Omega}{2}, \quad b = p + \frac{\ell\Omega}{2}, \quad c = 2p + 1 - \frac{3}{2}, \quad (18)$$

and the parameter p is determined by

$$4p^2 - 6p - \ell^2\mu^2 = 0 \rightarrow p_\pm = \left(3 \pm \sqrt{9 + 4\ell^2\mu^2}\right)\Big/4. \ (19)$$

The general solution to (17) is given in terms of the hypergeometric function $_2F_1(a, b, c; y)$ and reads

$$F(y) = C_1 \ _2F_1(a, b, c; y) + C_2 y^{1-c}$$
$$_2F_1(a - c + 1, b - c + 12 - c; y), \qquad (20)$$

where C_i, $i = 1, 2$ are integration constants. In general, this solution is not regular for $y \to 0$ unless $a = -k$, $k \in \mathbb{N}$. This leads to the following requirement for Ω:

$$\Omega = \frac{2(p+k)}{\ell}, \qquad k \in \mathbb{N}, \qquad (21)$$

i.e., Ω is quantized. Moreover, the solutions indexed by k possess k zeros. These provide the "gauged oscillon" basis that describes the solutions to the linearized equation (15). This oscillon basis has been discussed previously in the case of massless scalar fields [24,25] as well as including the mass of the scalar field [26].

We hence expect that solutions with zeros in the scalar field function exist also in the nonlinear case and would interpret them as radially excited solutions. In the following, we will demonstrate that these solutions can, indeed, be constructed numerically and agree with the analysis done above in the linear limit. Note that in the asymptotically flat case, $\Lambda = 0$, there is no equivalent linear argument. However, as we will demonstrate below, excited solutions do exist.

III. RESULTS

In order to solve the equations numerically it is convenient to rescale as follows:

$$m \to \frac{m}{\mu}, \qquad \Omega \to \mu\Omega, \qquad \Lambda \to \Lambda\mu^2,$$

$$\psi \to \eta\psi, \qquad V \to \eta V, \qquad (22)$$

and define the following dimensionless quantities:

$$x = \frac{r}{\mu}, \qquad e = \frac{\eta q}{\mu}, \qquad \alpha = 4\pi G\eta^2. \quad (23)$$

Solitonic solutions to the model given here have been previously constructed in the asymptotically flat case [17] (see also [18] for a very similar study, albeit with a sixth-order scalar potential) as well as in the ungauged case in aAdS [13]. Here, we will be interested in the influence of the charge on aAdS boson stars as well as radially excited solutions in both aAdS ($\Lambda < 0$) and asymptotically flat ($\Lambda = 0$) spacetime.

A. Unexcited solutions

As discussed above, we expect the model to possess solutions with nodes in the scalar field function. Here, we first discuss the solutions with no nodes, i.e., the solutions that are not radially excited, and will frequently refer to them as $k = 0$ solutions.

1. $\Lambda = 0$

Very similar to what has been discussed in [18] for a power-law scalar field potential, we find that also for the exponential scalar field potential three branches of solutions exist when plotting the diverse quantities versus $\Omega = \omega - e\Phi$ and choosing α and e appropriately. In the following, we will refer to these branches as branches A, B, and C, respectively, where branch A corresponds to the branch of lowest mass solutions for a given Ω and exists in the limit $\Omega \to 1$. In this limit the scalar field $\psi(r) \equiv 0$, while the mass M and Noether charge Q_N both approach a nonvanishing value. In Fig. 1, we show M and Q_N (left) as well as the value of the scalar field function at the origin, $\psi(r)$ (right) in function of Ω for $\alpha = 0.0012$ and $e = 0.02$. The three branches for the unexcited solution are clearly visible and we note that on all branches we have $M < Q_N$ indicating that the solutions on all branches are stable with respect to the decay into Q_N individual bosons of mass $\mu \equiv 1$. Moreover, we find that $M \to Q_N$ in the limit $\Omega \to 1$. The dependence of $\psi(0)$ on Ω [see Fig. 1 (right)] demonstrates that the central value of the scalar field cannot exceed a finite value. While on branch A the increase of $\psi(0)$ is connected to an increase of the Noether charge Q_N, i.e., the number of bosonic particles making up the boson star, this is no longer true for branch B. On this branch, the number of bosonic particles increases, but the central density decreases. This suggests that more and more bosonic particles are pushed out from the center due to the increased electromagnetic repulsion that the bosonic particles feel. On branch C finally, the
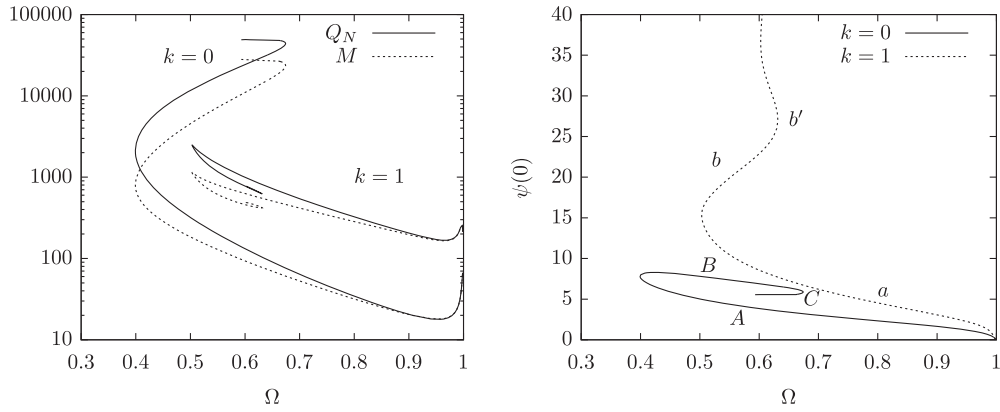
FIG. 1. Left: the dependence of the mass M (dashed) and Noether charge Q_N (solid) on Ω for unexcited boson stars ($k = 0$) as well as boson stars with one node in the scalar field function ($k = 1$), respectively. Here we have chosen $\alpha = 0.0012$, $e = 0.02$, $\Lambda = 0$. Right: the value of the scalar field at the origin $\psi(0)$ in function of Ω for the same solutions. A, B, C indicate the branches for $k = 0$ (solid), while a, b, b' refer to those for the $k = 1$ solutions (dashed).

value of $\psi(0)$ as well as the Noether charge Q_N stay more or less constant.

In order to understand this latter feature, let us discuss in more detail what happens on branch C. Again, this has been discussed previously for a power-law potential in

[18]. Here we show that this feature persists for the exponential potential and point out that the interpretation of results becomes easier when using ω instead of Ω. As argued in [18], the scalar field starts oscillating in regimes where the square of the effective mass $m_{\rm eff}$
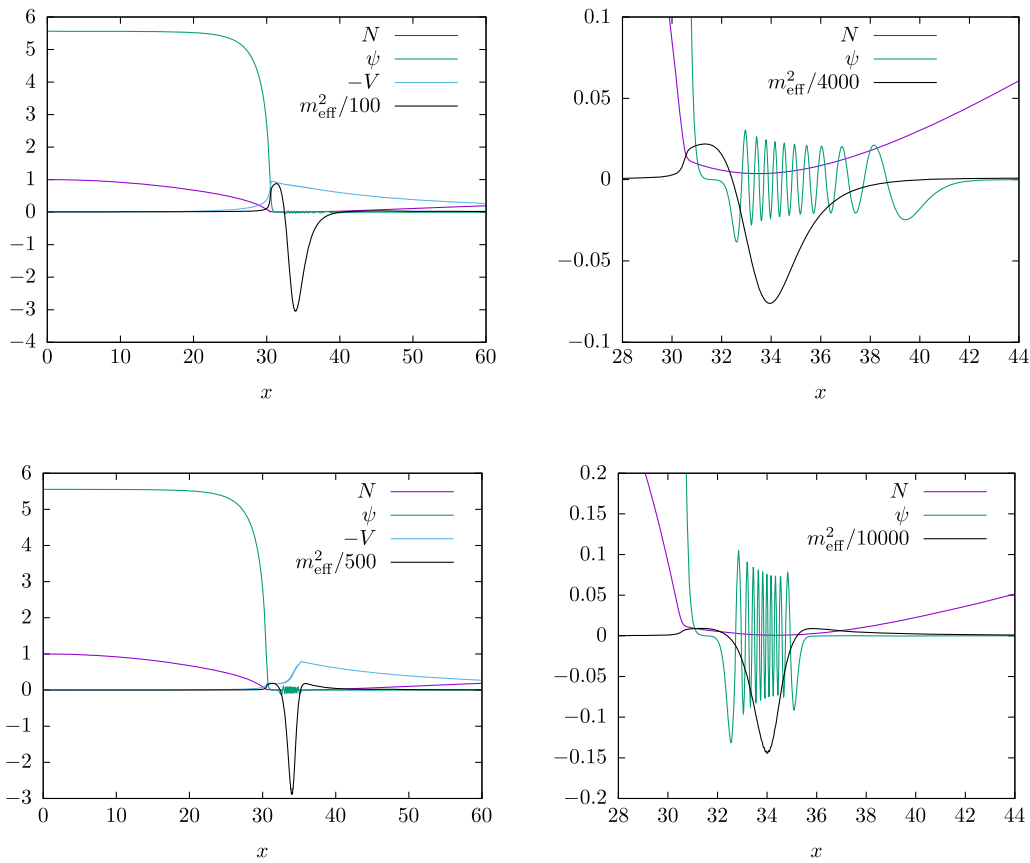

FIG. 2. We show the profiles of the metric function $N(x)$ (purple), scalar field function $\psi(x)$ (green), electric potential $-V(x)$ (light blue) (left only) as well as of the effective mass $m_{\rm eff}^2$ (black) [see (24)] for $\alpha = 0.0012$, $e = 0.02$, and $\omega = 0.001$ (upper row) as well as $\omega = 0.0002$ (lower row). The right figures in each row show an enlargement of the x-interval where $\psi(x)$ oscillates.
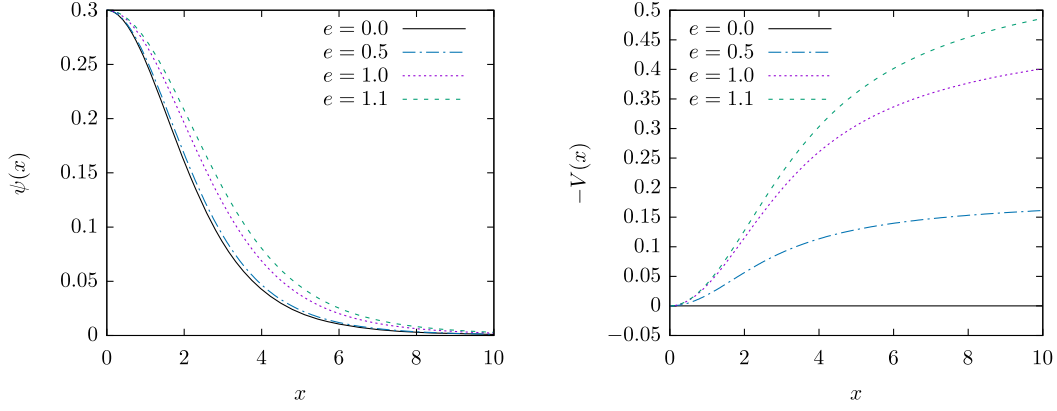
FIG. 3. Left: we show the scalar field function $\psi(x)$ of the unexcited solution ($k = 0$) for $\alpha = 0$, $\Lambda = -1/6$ and different values of the gauge coupling e: $e = 0$ (solid), $e = 0.5$ (dot-dashed), $e = 1.0$ (short dashed), and $e = 1.1$ (long dashed). Right: the corresponding gauge field function $-V(x)$.

defined by [note that $\mu \equiv 1$ due to our rescalings (22) and (23)]

$$m_{\text{eff}}^2(x) = \frac{1}{N(x)} - \frac{(\omega - eV(x))^2}{N^2(x)\sigma^2(x)} \qquad (24)$$

becomes negative. This is shown in Fig. 2 for $\alpha = 0.0012$, $e = 0.02$, and two different values of ω. We observe that when decreasing ω the value of the minimum of the metric function $N(x)$ decreases and in the limit $\omega \to 0$ tends to zero. We find, e.g., when decreasing ω from $\omega = 0.001$ to $\omega = 0.0002$ that the value of the minimum of $N(x)$ decreases from ≈ 0.004 to ≈ 0.0007. At the same time, the number of oscillations in the scalar field function stays constant (equal to 10 in our case), but the oscillations increase in amplitude and—at the same time—are squeezed to a smaller interval in x. This is clearly related to the fact that the effective mass m_{eff}^2 is more negative.

2. $\Lambda < 0$

In order to understand the influence of the charge on the solutions, we have first set $\alpha = 0$ (such that $N = 1 - \Lambda x^2/3$, $\sigma \equiv 1$) and studied the behavior of the solutions when varying e. This is shown in Fig. 3 for $e = 0$, 0.5, 1, and 1.1, corresponding to $\Omega \approx 1.40$, 1.47, 1.76, and 1.89, respectively. We observe that the scalar field function falls off slower when increasing e, which means a larger radius for the solitonic object. This is not surprising noticing that the configuration can be interpreted as being made of Q_N scalar and charged bosons, each charged with e. Increasing e hence increases the repulsion between the individual constituents and since the spacetime does not backreact, there is no attractive force to compensate for the repulsion. Hence, we cannot make a gauged scalar field object possess arbitrarily large scalar field values (as is, e.g., the case in flat spacetime in the ungauged case). This is demonstrated in Fig. 4 (left), where we give the value of the scalar field at the origin $\psi(0)$ in dependence of Ω for $\alpha = 0$,
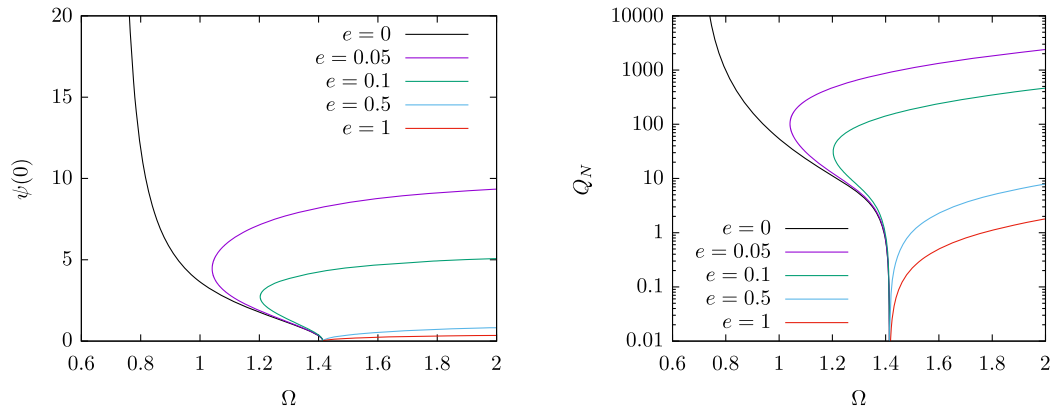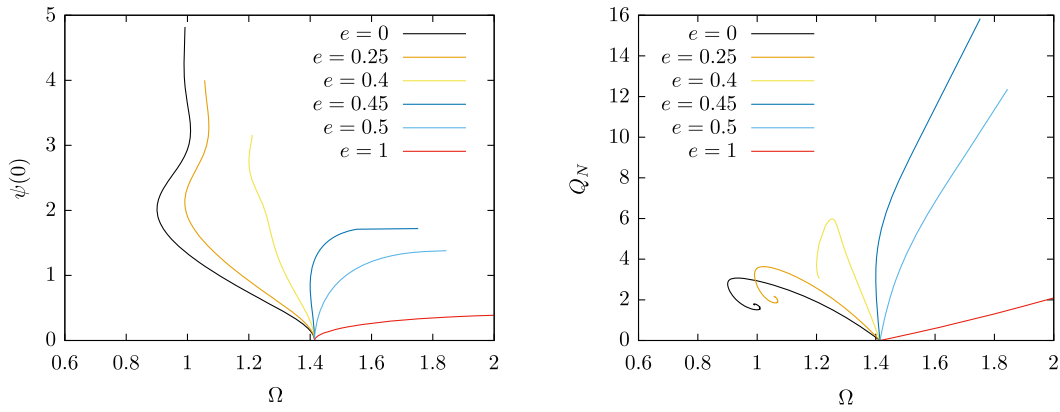

FIG. 4. Left: we show the value of the scalar field at the origin $\psi(0)$ as a function of Ω for $\alpha = 0$, $\Lambda = -1/6$, $k = 0$, and different values of e: $e = 0$ [black, not restricted in $\psi(0)$], $e = 0.05$ (purple), $e = 0.1$ (green), $e = 0.5$ (light blue), $e = 1$ (red) [with decreasing value of $\psi(0)$ at given Ω]. Right: the Noether charge Q_N as a function of Ω for the same solutions. Same color scheme with decreasing value of Q_N at Ω.

FIG. 5.   Left: we show the value of the scalar field at the origin $\psi(0)$ as a function of Ω for $\alpha = 0.1$, $\Lambda = -1/6$, $k = 0$, and different values of e: $e = 0$ (black), $e = 0.25$ (orange), $e = 0.4$ (yellow), $e = 0.45$ (dark blue), $e = 0.5$ (light blue), $e = 1$ (red)—from left to right. Right: the Noether charge Q_N as a function of Ω for the same solutions.

$\Lambda = -1/6$, and different values of e. For $e = 0$, the value of $\psi(0)$ can become arbitrarily large with the Noether charge $Q_N \to \infty$ [see Fig. 4 (right)]. Increasing e from zero, the behavior is qualitatively different. Solutions exist only down to a minimal value of Ω, where a second branch of solutions exists that extends backward in Ω with increasing values of $\psi(0)$ and Q_N. This means that the frequency Ω needs to increase in order for the gauged boson star to be composed of more bosonic particles. The larger e, the smaller is $\psi(0)$, which again can be explained by the increased electromagnetic repulsion.

To understand the influence of gravity, we give the values of ψ_0 and the Noether charge Q_N in dependence of Ω for $\alpha = 0.1$ in Fig. 5. Comparing this with the results for the $\alpha = 0$ case (see Fig. 4) the interplay between the electromagnetic repulsion and gravitational attraction becomes apparent. For $\alpha = 0.1$ the curve of $\psi(0)$ as a function of Ω does not show the above mentioned

backbending behavior until e is large enough. This is also seen when considering the Noether charge Q_N. For $e = 0$, $e = 0.25$, and $e = 0.4$ the curves show the typical spiraling behavior for uncharged boson stars. Only when the electromagnetic interaction becomes sufficiently strong and dominates the system does this behavior change. We also observe when comparing with the $\alpha = 0$ case that $\psi(0)$ is much larger when the backreaction of the spacetime is not taken into account. This is related to the fact that when the spacetime backreacts a limit for the mass of any gravitating object exists: $2M$ per Schwarzchild radius.

The branches A, B, and C discussed in the asymptotically flat case exist as well in the $\Lambda < 0$ case, see Fig. 6 (left), where we give $\psi(0)$ in function of ω for three different values of Λ including the already discussed asymptotically flat case. Clearly, the branches A, B, and C are present for $\Lambda < 0$ and the qualitative dependence of $\psi(0)$ on ω does not change significantly when changing Λ.
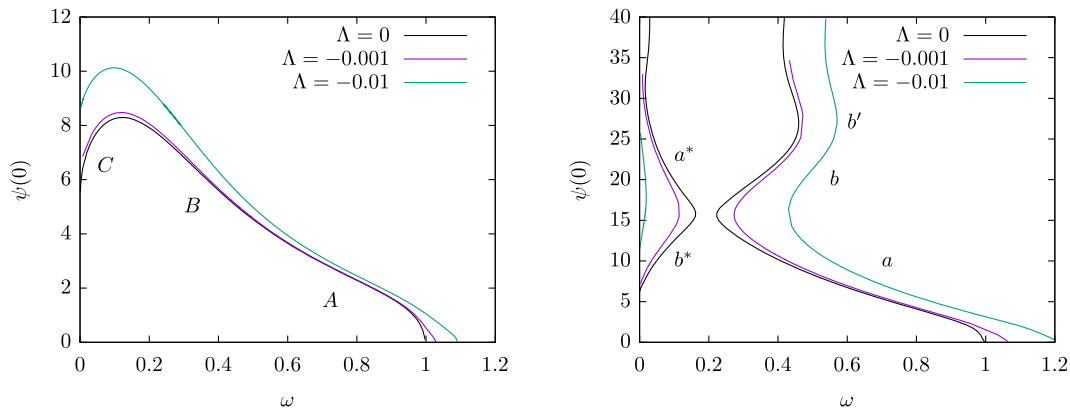

FIG. 6.   Left: we show the dependence of $\psi(0)$ on ω for the unexcited solution ($k = 0$) and three values of Λ indicating branches A, B, and C: $\Lambda = 0$ (black), $\Lambda = -0.001$ (purple), $\Lambda = -0.01$ (green)—with decreasing $\psi(0)$ at fixed ω. Right: we show the dependence of $\psi(0)$ on ω for the first radially excited solution ($k = 1$) and three values of Λ indicating branches a, b, b', and a^*, b^*, respectively, for three different values of Λ with the same color scheme as the left. For the data on the left and right we have chosen $\alpha = 0.0012$ and $e = 0.02$.
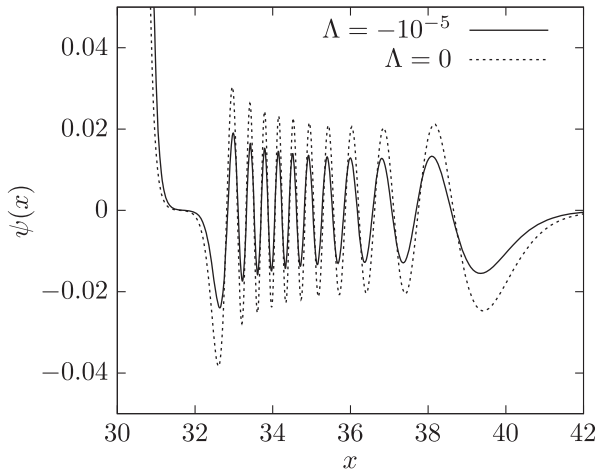
FIG. 7.   We show the profile of the scalar field function $\psi(x)$ for $\alpha = 0.0012$, $e = 0.02$, $\omega = 0.001$, and $\Lambda = 10^{-5}$ (solid) and $\Lambda = 0$ (dashed), respectively.

In fact, we find that the wavy scalar hair solutions discussed above also exist in the $\Lambda < 0$ case. In Fig. 7, we show the scalar field function for $\alpha = 0.0012$, $e = 0.02$, $\omega = 0.001$, and $\Lambda = 10^{-5}$ and compare it with the corresponding solution for $\Lambda = 0$ [see Fig. 2 (upper right)]. We observe that when changing Λ that the first three local maxima are slightly shifted to larger x, while the seven remaining maxima are slightly shifted to smaller values of x, i.e., the oscillations appear in a smaller interval of x. More significantly, however, we observe also that the amplitude of the oscillations decreases when decreasing Λ from zero. We would expect that decreasing Λ further, i.e., decreasing the AdS radius, will suppress the oscillations as soon as the AdS radius becomes comparable to the x-values at which these oscillations appear.

In order to make a connection to the AdS/CFT correspondence and the suggested interpretation of the field values of solitonic solutions in aAdS on the conformal
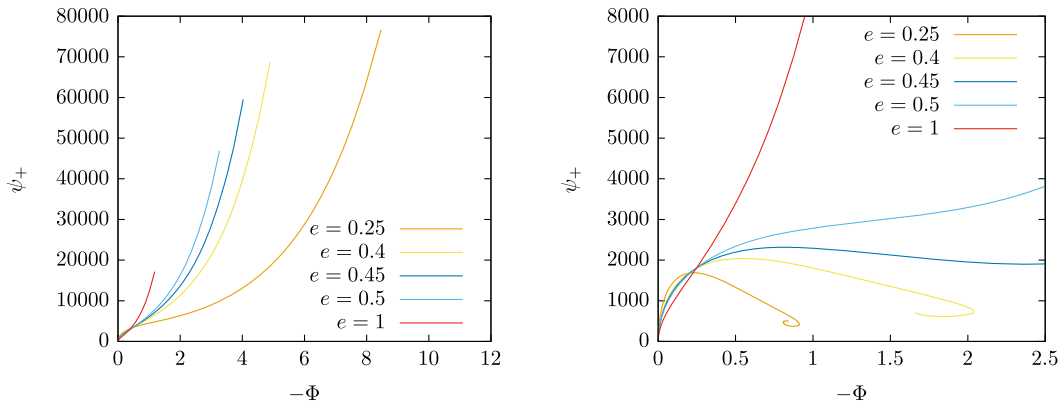

FIG. 8.   Left: the value of the condensate ψ_+ as a function of the chemical potential $-\Phi$ for several values of e, $\alpha = 0.01$, and $\Lambda = -1/6$: $e = 0.25$ (orange), $e = 0.04$ (yellow), $e = 0.45$ (dark blue), $e = 0.5$ (light blue), $e = 1$ (red) (from right to left). Right: same as left, but for $\alpha = 0.1$ with the same color scheme as the left, but with increasing values of ψ_+ at fixed $-\Phi$.
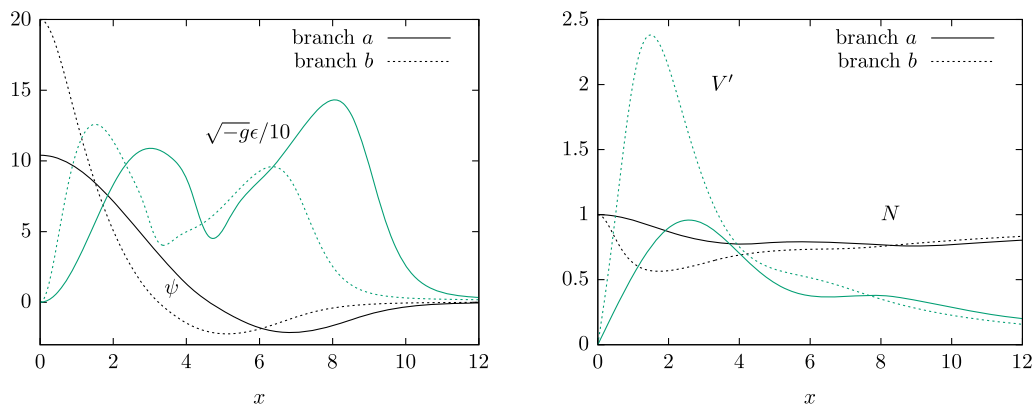

FIG. 9.   We compare the two radially excited solutions on branch a (solid) and branch b (dashed) for $k = 1$, $\alpha = 0.0012$, $e = 0.02$, $\Lambda = 0$, and $\Omega = 0.55$, see Fig. 1 (right). Left: scalar field function $\psi(x)$ (black, profile with node) and effective energy density $\sqrt{-g}T^0_0 = \sqrt{-g}\epsilon$ (green, profile with two local maxima). Right: metric function $N(x)$ (black, profile with value 1 at $x = 0$) and negative of electric field $V'(x)$ (green, profile with value 0 at $x = 0$.).

boundary in terms of glueball condensates (see, e.g., [4,13]), we plot the value of ψ_+ as a function of $-\Phi$ for $\Lambda = -1/6$, several values of e, and $\alpha = 0.01$ (left) and $\alpha = 0.1$ (right) in Fig. 8. This is hence a holographic phase diagram showing the condensate in function of the chemical potential. Increasing the backreaction of the spacetime, i.e., increasing α, changes the qualitative behavior of the condensate. At given fixed value of the gauge coupling e, the increase of the potential difference between the origin and the conformal boundary $V(0) - V(r \to \infty) = -\Phi$ increases the value of the condensate up to a maximal value of both the potential

difference and the condensate value. We observe that this is true for small α and e and find that the maximal possible value of the condensate decreases with increasing e and α. For larger values of α and sufficiently large values of e we observe that at a given value of $-\Phi$ the condensate reaches a maximum and then decreases again when increasing $-\Phi$ further. In fact, we find that for e large enough a spiraling behavior of the condensate value appears, i.e., we observe that for a given values of e and α an interval in $-\Phi$ exists on which different values of the condensate are possible for the same value of $-\Phi$.
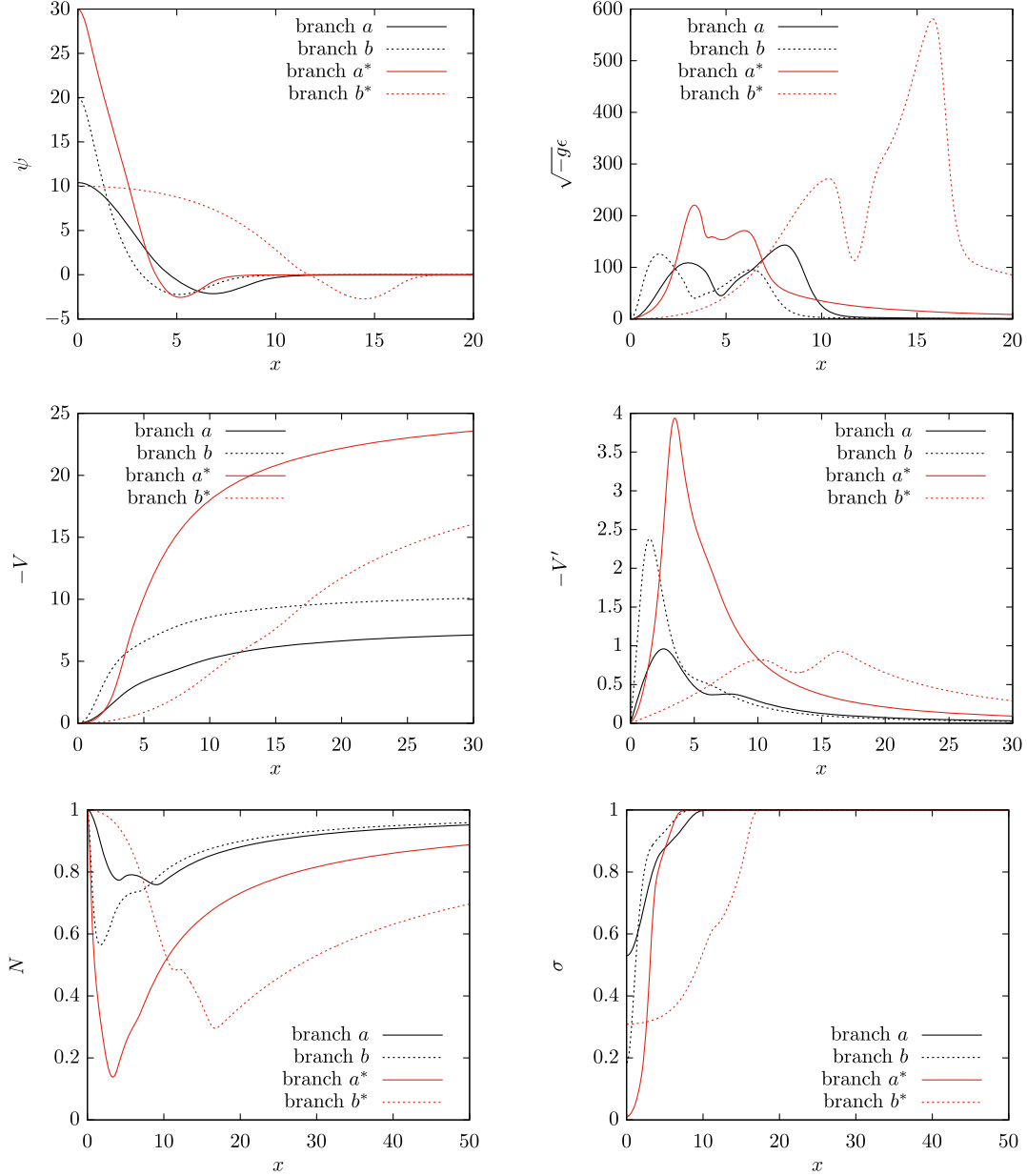

FIG. 10.   We compare the four radially excited solutions on branches a (solid black), b (dashed black), a^* (solid red), and b^* (dashed red) for $k = 1$, $\alpha = 0.0012$, $e = 0.02$, $\Lambda = 0$, and $\Omega = 0.53$, see Fig. 6. Top left: scalar field function $\psi(x)$. Top right: effective energy density $\sqrt{-g}T_0^0 = \sqrt{-g}\epsilon$. Middle left: electric potential $-V(x)$. Middle right: electric field $-V'(x)$. Bottom left: metric function $N(x)$. Bottom right: metric function $\sigma(x)$.
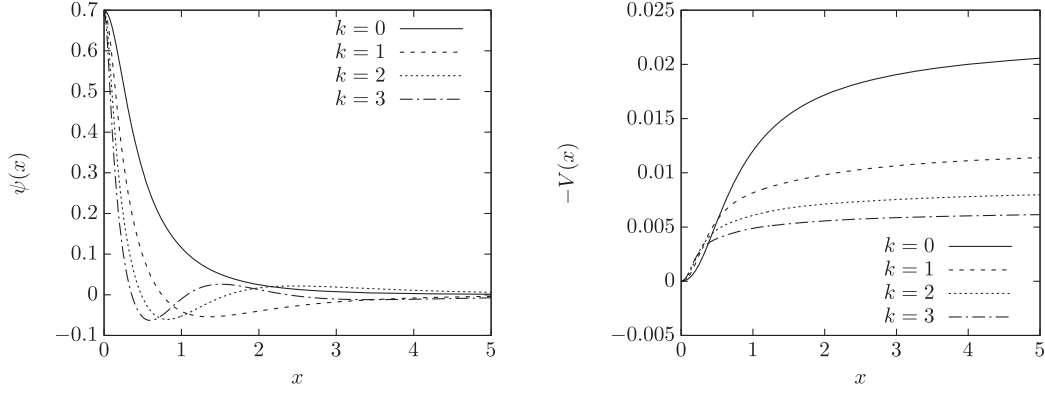
FIG. 11. Left: we show the scalar field function $\psi(x)$ of the unexcited solution ($k = 0$, solid) and the first three radially excited solutions [$k = 1$ (dashed), $k = 2$ (dotted), $k = 3$ (dot-dashed)] for $\alpha = 1$, $e = 0.1$, and $\Lambda = -3/4$. Right: the corresponding gauge field function $-V(x)$.

B. Radially excited solutions

Following our discussion above, we would expect that radially excited boson stars in aAdS should exist in our model. In fact, they also exist for the $\Lambda = 0$ limit and since these solutions have not been discussed in the literature so far, we will first present our results for the asymptotically flat case.

1. Λ = 0

In Fig. 1, we show the mass M and the Noether charge Q_N of the radially excited boson stars with one node in the scalar field function ($k = 1$) for $\alpha = 0.0012$ and $e = 0.02$ in dependence on Ω. We find that the unexcited and the one-node solutions show a qualitatively similar behavior in the limit $\psi(0) \to 0$, e.g., $\Omega \to 1$ for both $k = 0$ and $k = 1$ and the scalar field function tends uniformly to zero while the mass M and Noether charge Q_N tend to nonvanishing values.

The behavior, however, changes when increasing $\psi(0)$. While we also find several branches for the radially excited case (see Fig. 9 for a typical profiles of such a solution), these have very different features as compared to the branches discussed for $k = 0$. Rather than finding branches A, B, and C, the excited solutions form several branches in

the form of a spiral for which we will use the labels a, b, and b' (for the first three branches) in the following. In fact, the second branch of excited solutions has lower mass and Noether charge, respectively, as the first major branch that connects to $\Omega = 1$. To understand this result, we show the scalar field and the associated effective energy density $\sqrt{-g}T^0_0 = \sqrt{-g}\epsilon$ in Fig. 10 (upper row) for $\Omega = 0.55$ and the branches a and b. We observe that the solutions on branch b have a larger central value of the scalar field $\psi(0)$, but that the scalar field's node is at smaller x. Moreover, we find that the effective energy density possesses two local maxima, one close to the node of the scalar field function. These maxima are more pronounced for solutions on branch a.

In Fig. 10 (middle row), we show the electric potential $V(x)$ and the electric field $-V'(x)$ for the same solutions. Both potential and electric field are stronger close to the core of the boson star for the solutions on branch b as compared to those on branch a. Consequently, the local spacetime curvature is also stronger there, see the metric functions $N(x)$ and $\sigma(x)$ in Fig. 10 (bottom row).

Interestingly, we find that, next to the branch of solutions discussed above, another, completely disconnected branch
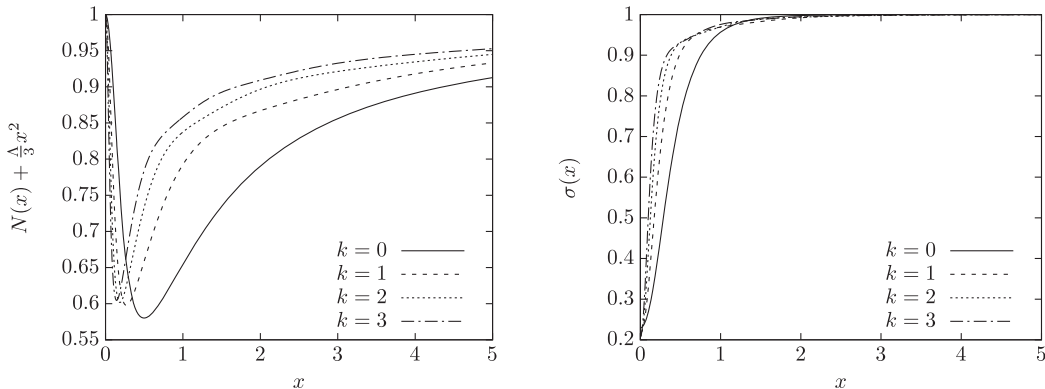

FIG. 12. We show the metric function $N(x) + \frac{\Lambda}{3}x^2$ of the unexcited solution ($k = 0$, solid) and the first three radially excited solutions [$k = 1$ (dashed), $k = 2$ (dotted), $k = 3$ (dot-dashed)] for $\alpha = 1$, $e = 0.1$, and $\Lambda = -3/4$. Right: the corresponding metric function $\sigma(x)$.
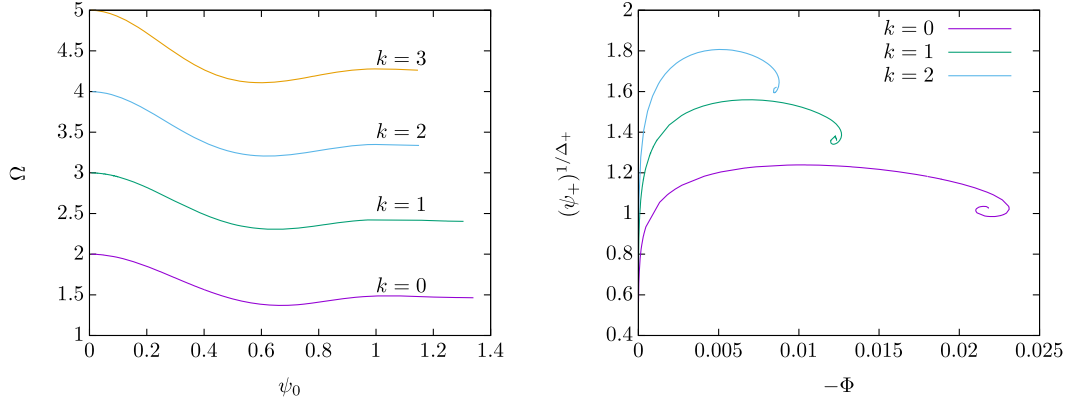
FIG. 13.   Left: we show the value of Ω in dependence of the value of the scalar field function at the origin ψ_0 of the unexcited solution ($k=0$) (purple) [$k=1$ (green), $k=2$ (light blue), $k=3$ (orange)] and the first three radially excited solutions ($k=1,2,3$) for $\alpha=1$, $e=0.1$, and $\Lambda=-3/4$. Right: the corresponding condensate $(\psi_+)^{1/\Delta_+}$ as a function of the chemical potential $-\Phi$ for $k=0,1,2$ with the same color scheme as the left and decreasing value of $(\psi_+)^{1/\Delta_+}$ at fixed $-\Phi$.

exists that appears only in the highly nonlinear regime. This is shown in Fig. 6 (right) where we give the value of $\psi(0)$ in dependence on ω. To compare, we have also plotted again the values for the branches a, b, and b'. At sufficiently small ω and sufficiently large $\psi(0)$, we find two new branches a^* and b^* that are disconnected from the other branches and do not connect to the $\omega=1$, $\psi(0)=0$ limit. In keeping with the notation used above, the b^* part of these new solutions has higher mass as compared to the a^* part.

In order to understand the difference between these one-node solutions, we show the scalar field function $\psi(x)$ as well as the effective energy density $\sqrt{-g}\epsilon$ of the four $k=1$ solutions for $\Omega=0.53$ in Fig. 10 (upper row), the corresponding electric potential $V(x)$ and field $-V'(x)$, respectively, are shown in Fig. 10 (middle row), while we give the metric functions $N(x)$ and $\sigma(x)$, respectively, in Fig. 10 (bottom row). Interestingly, branches a, b, and a^* have the zero of the scalar field function roughly at the same value of x, while the zero of the solution on branch b^* is at much larger values of x. The corresponding maximum of the effective energy density $\sqrt{-g}\epsilon$ as well as the minimum of the metric function $N(x)$ consequently also appear at larger x for branch b^* as compared to the remaining branches.

2. $\Lambda < 0$

We have constructed these solutions numerically. In Figs. 11 and 12, we show the matter and metric functions, respectively, of solutions with $k=1$, 2, and 3 zeros in the scalar field function corresponding to $\Omega \approx 2.32$, 3.23, and 4.15, respectively, for $\alpha=1$, $e=0.1$, and $\Lambda=-3/4$. Increasing k, we observe that the minimum of the metric function $N(x)$ decreases in value and moves closer to the origin, while $\sigma(x)$ reaches its asymptotic value quicker when increasing k.

In Fig. 13 (left), we give Ω as a function of the scalar field function at the origin $\psi(0) \equiv \psi_0$ for solutions with $k=0,1$,

2, and 3 nodes in the scalar field for $\mu=1$ and $\Lambda=-3/4$. Using the discussion on oscillons (see Sec. II A), we have hence $p_+ = 2$ and consequently $\Omega = 2+k$, $k \in \mathbb{N}$. The data in Fig. 13 clearly demonstrate that for small values of ψ_0 we find that $\Omega = 2+k$, where k is the number of nodes of the scalar field function in agreement with the discussion given above. Increasing ψ_0 leads to a decrease in the value of Ω until $\Omega_{\min}$ is reached at some intermediate value of ψ_0. We find that Ω reaches its minimal value at decreasing values of ψ_0 when increasing the number of nodes in the scalar field.

In Fig. 13 (right), we give the value of the condensate, i.e., the value of the scalar field on the conformal boundary $(\psi_+)^{1/\Delta_+}$ in function of the chemical potential $-\Phi$. For all k we find that the condensate builds up strongly when increasing $-\Phi$ from zero. It then reaches a maximal value and this is attained at decreasing values of $-\Phi$ when increasing k. The condensate then decreases up to a maximal value of $-\Phi$ and starts to form a spiral with several branches appearing. We observe a similar behavior for all k, but note that the interval in $-\Phi$ for which solutions exist decreases with k. Interestingly, we also find that the value of the condensate increases when increasing k at a fixed chemical potential and that different values of the condensate are possible for sufficiently large and fixed $-\Phi$.

Interestingly, we find that the new branches of solutions found in the $\Lambda=0$ limit exist as well for $\Lambda < 0$, at least as long as Λ is sufficiently close to zero. This is shown in Fig. 6 (right). The branches a, b, and b' move to larger values of ω, while the branches a^* and b^* move to smaller values of ω. For $\Lambda = -0.01$, the a^* and b^* branches have nearly disappeared. Hence, these branches exist only for Λ sufficiently close to zero.

IV. CONCLUSIONS

In this paper, we have studied electrically charged boson stars with an exponential scalar field interaction in asymptotically flat and anti–de Sitter spacetime, respectively.

Next to the standard boson stars discussed in the literature previously, we find several new branches of solutions. For the unexcited solutions ($k = 0$), i.e., solutions without nodes in the scalar field function inside the boson star core, we observe that the formation of wavy scalar hair on the boson stars discussed before in asymptotically flat spacetime [18] also exists in aAdS spacetime, at least for small values of $|\Lambda|$. This hair appears for gravitational interaction sufficiently large and electromagnetic interaction sufficiently small and involves the splitting of the spacetime into a "false vacuum" interior (where the scalar field is constant, but nonzero) and a "true vacuum" exterior (where $\psi \equiv 0$). The interior hence corresponds to a de Sitter spacetime with the constant scalar field leading to a constant positive potential energy that can be interpreted as a positive cosmological constant. The exterior corresponds to a spacetime without scalar field, i.e., an extremal Reissner-Nordström(-AdS) solution. At the intersection between these spacetimes, the scalar field starts oscillating.

When considering radially excited solutions, we find that the wavy scalar hair is not present, which also confirms that the spatial oscillations interpreted as wavy scalar hair are *not* radial excitations of the boson star. In fact, we observe a qualitatively very different behavior. When increasing the central value of the scalar field, instead of reaching a maximal possible value as in the $k = 0$ case, we find that the central value can become much larger and seems (at least within our numerical analysis) not to be bounded from above as soon as the boson star is radially excited. Moreover, we have constructed new branches of radially excited solutions that seem disconnected from the linear scalar field limit and seem to be a truly nonlinear phenomenon. These branches disappear when decreasing Λ too strongly from zero, i.e., exist only when the AdS radius is sufficiently large.

Within the context of the holographic interpretation, we find that the radially excited solutions can produce larger values of the condensate, i.e., the scalar field value on the conformal boundary, as compared to the unexcited solutions. In order to get a better understanding of these condensates, it will be interesting in the future to construct the corresponding black hole solutions and find holographic phase diagrams. This is currently under investigation.

Finally, let us make a few comments on the stability of the newly found solutions. Radial excitations are often associated with instabilities, however, in particular in physical systems that possess nonlinear interactions, this connection does not always hold true. Moreover, different notions of stability appear in nonlinear models. There is linear stability versus dynamical stability and also different notions of stability that rely on comparing the mass of the solutions to that of other possible states in the system. As an example, let us mention AdS spacetime itself that is linearly stable, but dynamically unstable to the formation of black holes [24]. In the context of boson stars, one often compares the mass M of the boson star with that of an assembly of Q_N scalar bosons of mass m. If $M < mQ_N$ the boson star is stable against decay into Q_N scalar bosons, i.e., forms a bound state of these entities. All new solutions we have discussed in this paper are stable in this sense for sufficiently large Q_N. Only for small Q_N and no nodes in the scalar field function can the boson stars have $M > mQ_N$. This latter result, however, is well known and has been discussed extensively before. When discussing the dynamical stability of boson stars, it has been shown in [27] that uncharged boson stars in asymptotically flat spacetime are dynamically stable only up to a maximal value of the central density $\psi(0)$. Now, when discussing charged boson stars the situation is different since charged boson stars cannot possess arbitrarily large central density (in contrast to uncharged boson stars) due to the electromagnetic repulsion between the charged scalar bosons making up the boson star. Hence, a more detailed numerical analysis that goes beyond the scope of this paper would be necessary. Now, considering the aAdS case, it was shown in [28] that the unexcited and the first three excited uncharged boson stars are dynamically stable—a clear counterexample to the statement that excited solutions in nonlinear settings are unstable. In summary, while the argument of the decay into individual scalar bosons demonstrates that the new solutions discussed in this paper are stable in this sense, the discussion of the dynamical (in)stability needs a more detailed numerical analysis in the future.

[1] J. M. Maldacena, The large N limit of superconformal field theories and supergravity, Adv. Theor. Math. Phys. **2**, 231 (1998).

[2] see, e. g., O. Aharony, S. S. Gubser, J. M. Maldacena, H. Ooguri, and Y. Oz, Large N field theories, string theory and gravity, Phys. Rep. **323**, 183 (2000); E. D'Hoker and D. Z. Freedman, Supersymmetric gauge theories and the AdS/CFT correspondence, arXiv:hep-th/0201253; M. Benna and I. Klebanov, Gauge-string duality and some applications, arXiv:0803.1315.

[3] S. A. Hartnoll, C. P. Herzog, and G. T. Horowitz, Building a Holographic Superconductor, Phys. Rev. Lett. **101**, 031601

(2008); Holographic superconductors, J. High Energy Phys. 12 (2008) 015; G. T. Horowitz and M. M. Roberts, Holographic superconductors with various condensates, Phys. Rev. D **78**, 126008 (2008).

[4] G. T. Horowitz and B. Way, Complete phase diagrams for a holographic superconductor/insulator system, J. High Energy Phys. 11 (2010) 011.

[5] S. R. Coleman, Q-balls, Nucl. Phys. **B262**, 263 (1985).

[6] A. Kusenko, Small Q balls, Phys. Lett. B **404**, 285 (1997).

[7] E. J. Copeland and M. I. Tsumagari, Q-balls in flat potentials, Phys. Rev. D **80**, 025016 (2009).

[8] D. J. Kaup, Klein-Gordon geon, Phys. Rev. **172**, 1331 (1968).

[9] R. Friedberg, T. D. Lee, and Y. Pang, Scalar soliton stars and black holes, Phys. Rev. D **35**, 3658 (1987).

[10] P. Jetzer, Boson stars, Phys. Rep. **220**, 163 (1992).

[11] F. E. Schunck and E. W. Mielke, General relativistic boson stars, Classical Quantum Gravity **20**, R301 (2003).

[12] D. Astefanesei and E. Radu, Boson stars with negative cosmological constant, Nucl. Phys. **B665**, 594 (2003).

[13] B. Hartmann and J. Riedel, Glueball condensates as holographic duals of supersymmetric Q-balls and boson stars, Phys. Rev. D **86**, 104008 (2012).

[14] P. Jetzer and J. J. van der Bij, Charged boson stars, Phys. Lett. B **227**, 341 (1989).

[15] H. Arodz and J. Lis, Compact Q-balls and Q-shells in a scalar electrodynamics, Phys. Rev. D **79**, 045002 (2009).

[16] B. Kleihaus, J. Kunz, C. Lämmerzahl, and M. List, Charged boson stars and black holes, Phys. Lett. B **675**, 102 (2009).

[17] Y. Brihaye, V. Diemer, and B. Hartmann, Charged Q-balls and boson stars and dynamics of charged test particles, Phys. Rev. D **89**, 084048 (2014).

[18] Y. Brihaye and B. Hartmann, Boson stars and black holes with wavy scalar hair, Phys. Rev. D **105**, 104063 (2022).

[19] D. Pugliese, H. Quevedo, J. A. Rueda H., and R. Ruffini, On charged boson stars, Phys. Rev. D **88**, 024053 (2013).

[20] B. Kleihaus, J. Kunz, and M. List, Rotating boson stars and Q-balls, Phys. Rev. D **72**, 064002 (2005).

[21] A. Bernal, J. Barranco, D. Alic, and C. Palenzuela, Multistate boson stars, Phys. Rev. D **81**, 044031 (2010).

[22] L. A. Urena-Lopez and A. Bernal, Bosonic gas as a galactic dark matter halo, Phys. Rev. D **82**, 123535 (2010).

[23] L. G. Collodel, B. Kleihaus, and J. Kunz, Excited boson stars, Phys. Rev. D **96**, 084066 (2017).

[24] P. Bizon and A. Rostworowski, On Weakly Turbulent Instability of Anti–de Sitter Space, Phys. Rev. Lett. **107**, 031102 (2011).

[25] O. J. C. Dias, G. T. Horowitz, D. Marolf, and J. E. Santos, On the nonlinear stability of asymptotically anti–de Sitter solutions, Classical Quantum Gravity **29**, 235019 (2012).

[26] Y. Brihaye, B. Hartmann, and J. Riedel, Self-interacting boson stars with a single Killing vector field in anti–de Sitter space-time, Phys. Rev. D **92**, 044049 (2015).

[27] M. Gleiser, Stability of boson stars, Phys. Rev. D **38**, 2376 (1988).

[28] A. Buchel, S. L. Liebling, and L. Lehner, Boson stars in AdS spacetime, Phys. Rev. D **87**, 123006 (2013).